Molecular dynamics study of the lauryl alcohol-laurate model bilayer

T. Fukada, S. Okazaki, and I. Okada
Department of Electronic Chemistry, Tokyo Institute of Technology, Midori-ku, Yokohama 227, Japan

ABSTRACT Molecular dynamics (MD) calculation of the fluid phase lauryl alcohol–laurate bilayer has been executed based on Berendsen's surface-constrained model. Structure and dynamics of the bilayer have been investigated by analyzing the trajectories of the chain configurations. Newly defined correlation functions as well as the conventional ones showed that the tilt and bend of the chain play an important role in the bilayer structure, including behavior of the order parameter. Interpenetration of the layers as well as formation of collectively ordered small domains was also found. The calculated lateral diffusion coefficient was in satisfactory agreement with the experimental one. Successive jumps of the head group, rather than the hydrodynamic continuous motion, were observed. Between the jumps, the molecule librated in a local site. Time-dependent autocorrelation functions showed evidence of several different modes of the chain motion, whose time constant ranged from a few tenths of picoseconds to several tens of picoseconds.

INTRODUCTION

A huge number of experimental and theoretical investigations have been done on lipid bilayers as model systems of cell membranes and organelles that play an indispensable role in biosystems. The experimental works consist mainly of thermodynamic (1), spectroscopic (2), and diffraction (3, 4) measurements combined with biochemical processes including both static and dynamic properties. The former is concerned with stability of phases of the bilayers and their phase structures, related to, for example, order–disorder structure, ripple, and tilt, and the latter with the motion of the bilayers or lipid chains, phase transition, and material transportation across the membranes, et cetera. However, based on the conformations of the alkyl chains, the structural studies of the membranes in fluid and gel phases seem to belong a semimacroscopic overview rather than a microscopic fine structure. The only exceptions are the crystal phase, where the detailed structure including the conformations can be obtained by a diffraction technique (3), and an order parameter analysis based on nuclear magnetic resonance (NMR) bandwidth measurement (4). With regard to the dynamics, nanosecond or longer dynamics has been investigated, for example, for tilt, bend, and lateral diffusion of the lipid chain and for the transportation of materials across the layers. However, there has been little knowledge of more rapid motion of the chain, i.e., on the order of picoseconds.

A number of statistical mechanical models have been proposed (5–8) so far to understand the microscopic structure of the fluid phase of lipid bilayers. In principle, most of them are concerned with the packing of the chain into a volume with simple intermolecular interactions. However, the statistical model as well as the potential function adopted is too primitive to reproduce well the static properties of the bilayers. The membrane is too complex to be represented by such simple models. The dynamic properties cannot be analyzed by such kinds of statistical models.

In the present work, molecular dynamics (MD) calculations have been performed for a lauryl alcohol–laurate model bilayer to explore the static and dynamic properties of the real membrane in a microscopic view. The first MD calculation of the bilayer was reported by Berendsen's group about 10 years ago (9, 10). To our knowledge, however, after their pioneering reports, the simulation study was not developed until a few recent similar calculations (11–13). This is probably because the membrane systems are so large that the calculations require enormous computation time, even with the use of recent vector computers.

Two kinds of bilayer models have been proposed by Berendsen's group. In the first calculations (9, 10), water molecules were not contained in the system, where a role of the solvent to form a bilayer such as hydrophobic interaction was replaced by the direct harmonic potential along the bilayer normal between the united head group and the wall. Another model (11) accommodated cations and water molecules, where the head group had a fine structure constructed by atoms. The latter model was, in principle, superior physically to the former. These two MD calculations were successful in their own ways and threw light on the investigation of the fine structure and dynamics of membranes, which could not be clarified by experiments alone.

However, the scale of their calculated systems was still small, i.e., 64×2 lipid molecules, although the artifacts found in their previous 16×2 system do not appear there. In particular, in the case of the system containing water, some peculiar phenomena that seem not to occur in reality were observed, probably because of a too-small number of solvent water molecules as well as the approximation in the calculation of long-range coulombic force; that is, a zigzag structure of charged decanoate and neutral decanol, disappearance of electric double layer, and direct bonding of Na^+ ion with decanoate ions on

Address correspondence to Dr. Susumu Okazaki, Department of Electronic Chemistry, Tokyo Institute of Technology, 4259 Nagatsuta, Midori-ku, Yokohama 227, Japan.

0006-3495/93/04/1344/10 $2.00

both layer sides occurred. Of course, it is difficult as well as time consuming to learn how many water molecules are sufficient to reproduce the real membrane system. Furthermore, the period of their MD calculation was limited within 80 ps, which is a little too short to investigate a long-time-scale motion of the lipid molecule such as tilt and lateral diffusion.

In the present work, a large-scale MD calculation has been performed to study relatively long-time-scale motion of the lipid, and to avoid the artifacts caused by a small number of molecules. The surface-constrained model (9, 10) was adopted here to investigate the structure and dynamics of the lipid bilayer in the fluid phase already formed rather than to study why the bilayer is stably constructed in water. The number of lipid molecules is $100 \times 2 = 200$ (2,400 particles), which is about twice the magnitude of the system studied by Berendsen's group. The MD period was totally 390 ps including the equilibration time. This enables us to discuss the motion of the membrane whose time scale is, at least, longer than several tens of picoseconds.

In the rest of the paper, the present calculations and the potential model are roughly described. Structure and dynamics of the bilayer and its component lipid molecules are discussed in detail by newly defined static and time-dependent correlation functions as well as by perspective and projected pictures. A comparison with the work by Berendsen's group is also made.

CALCULATION

MD calculation

The MD calculation has been performed in NVT ensemble with the leap-flog algorithm (14) using our original program. A united atom model was adopted here for alkyl chain and COO^- group ($m_{CH_2} = 14$, $m_{CH_3} = 15$, $m_{COO^-} = 44$) because the motion of hydrogen atoms of the alkyl chain is beyond our present concern. During the calculation, the C—C bond length was always fixed by the SHAKE method (15). A unit cell contained two layers of 100 laurate (dodecanoate) molecules, $CH_3(CH_2)_{10}COO^-$, i.e., 2,400 particles, in the periodic boundary condition in two directions x and y, i.e., bilayer lateral. In the present calculation, lauryl alcohol molecule was not distinguished from laurate molecule, following the surface-constrained model (9). The periodic boundary condition was not adopted to z-direction, i.e., bilayer normal. The cell size was $50 \times 50 \times 23$ Å, where the lateral dimension was determined based on the experimental data for a decanol-decanoate–water system (16), whereas the dimension normal to the bilayer was adjusted in the calculation to reproduce the pressure in the longitudinal direction as stated below. The density of the system was 1.1 g/cm^3 and the surface number density of the head group was 0.04/Å^2. Temperature was maintained by Berendsen's method (17) with a response time of 1 ps. The time step was 5 fs, which was short enough to preserve the total energy in a preliminary MD run in NEV ensemble.

After a long equilibration run (180 ps) from the initial all-*trans* configuration with the molecular axes normal to the bilayer, the MD run was continued for further 210 ps at $T = 310$ K to obtain various kinds of static and dynamic functions. In the first 150 ps of equilibration, bilayer thickness was decreased from 31 to 23 Å, probably because of the tilt of the chains. Averaged lateral pressure was 4.8 MPa, whereas longitudinal pressure was −2.8 MPa. Although the value of the pressures is somewhat different from atmospheric 0.1 MPa, the order is in good accord with that in the real system. The present pressure value is satisfactory, considering the fact that MD pressure is always too sensitive to the potential function to reproduce the experimental PVT curve, and the physical properties of the layer are insensitive to the pressure of this order. Averaged total energy was ~11 kJ/mol with a fluctuation of roughly 1 kJ/mol in our NVT ensemble. Total MD run (78,000 steps) required ~15 h by the HITAC S-820 super computer at the Institute of Molecular Science.

Potential model

The interaction model is almost the same as that of van der Ploeg and Berendsen (9). First, bond angle potentials are taken as harmonic function

$$V(\theta) = (1/2)k_a(\theta - \theta_0)^2, \quad (1)$$

where $k_a = 520$ kJ · mol^{-1} · rad^{-2} was derived from a potential function used by Weber (18) ($\theta_0 = 1.9106$ rad.).

Dihedral potential function is

$$V(\phi) = \sum_i C_i(\cos\phi)^i, \quad (2)$$

with $C_0 = 1{,}116\,k_B$, $C_1 = 1{,}462\,k_B$, $C_2 = -1{,}578\,k_B$, $C_3 = -368\,k_B$, $C_4 = 3{,}156\,k_B$, and $C_5 = -3{,}788\,k_B$ (19), where k_B is the Boltzmann constant. This causes *trans*-gauche barrier energy = 12.3428 kJ/mol, and energy of the gauche minimum = 2.9288 kJ/mol. Hereafter, we refer to $-\pi/3 \le \phi \le \pi/3$ as *trans* conformation, which is abbreviated as t, $-\pi \le \phi < -\pi/3$ as g^-, and $\pi/3 < \phi \le \pi$ as g^+.

The Lennard-Jones interaction between all intermolecular pairs and those intramolecular pairs (i, j) for which $j > i + 3$ is

$$V(r_{ij}) = 4\epsilon[(\sigma/r_{ij})^{12} - (\sigma/r_{ij})^6]. \quad (3)$$

There are three types of particles; CH_2, CH_3, and COO^-. For ϵ and σ of CH_2, the literature values of 0.4301 kJ/mol and 3.74 Å, respectively, (20) were adopted. For CH_3 ϵ and σ were 0.6423 and 2.74, respectively, and for COO^- 0.9203 and 4.22 (21). The Lorentz-Berthelot combination rule (22) was used for cross-interactions. The interaction cut-off radius of 15 Å was used.

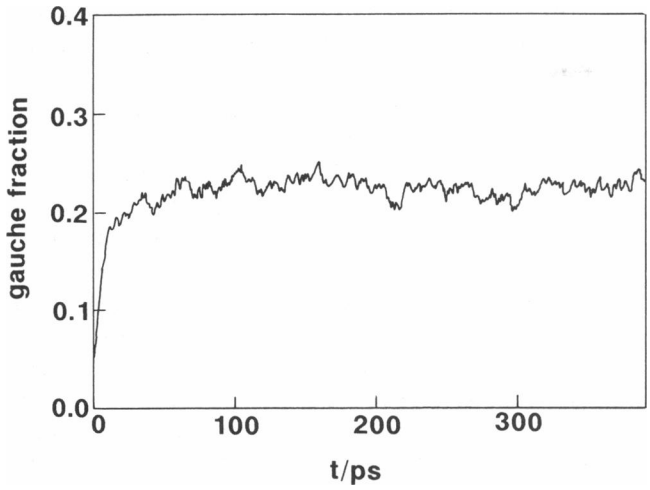

FIGURE 1 Convergence of gauche fraction from the initial condition of the MD run. The period when $t < 180$ ps was an equilibration run.

Interaction of head group units with the water layer is replaced by harmonic potential with the x-y plane wall

$$V(z) = (\frac{1}{2})k_h(z - z_0)^2 \quad (4)$$

The value of k_h is 3.00 kJ · mol^{-1} · Å^{-2}, and $z_0 = 0$ and 23 Å for each layer. In addition, it acts on all atoms of the chain, when the atom is outside the wall. This prevents the phenomenon that a molecule occasionally turns its tail outside the bilayer (9).

RESULTS AND DISCUSSION

Static properties

Fig. 1 shows time evolution of gauche fraction of the total system from the initial configuration of the present MD. Although gauche conformation increased rapidly from all-*trans* initial condition, roughly 60–100 ps of equilibration time was required to reach a stationary value and fluctuate around it. In contrast with an ordinary small-molecule system, this time is considerably long owing to the long chain. The fluctuation is rather small after reaching the equilibrium, i.e., ~0.02. All the ensemble averages of physical quantities were made after 180 ps of equilibration time, which is more than enough considering much shorter relaxation time from the initial configuration typically shown in this figure.

The system was in the fluid phase, as discussed later in detail. Calculated dihedral angle distribution of the lipid chain conformation in the fluid phase is compared with the distribution in a vacuum in Fig. 2. The integrated value was 0.22 and 0.34 for gauche conformation in the bilayer and in a vacuum, respectively, widths of the peaks being almost the same for these two. The gauche fraction was ~35% lower in the former than in the latter. The decrease has been observed also in the decanoate system by van der Ploeg and Berendsen (9) (0.21, 300 K) and in theoretical model calculation by Marsh (23) (0.22, 310 K). On the contrary, an increase in gauche conformation has been reported by Padrilla and Toxvaerd (24). The difference may be caused mainly by the packing of molecules. A gauche orientation of the long chain molecule often leads to a considerably bulky conformation, which hardly occurs in the dense phase. The chains are likely to align with each other to form *trans* conformation, i.e., to construct a layer. On the other hand, in the case of *n*-pentane, the volume change is not so large because the chain length is short. Other many-body interaction effects that relatively stabilize gauche conformation may be larger than the volume effect. The conformation in which $|\phi| > 0.89\pi$ ($\approx 160°$) was not observed because of the unfavorable potential energy either in the bilayer or in a vacuum.

The order parameter, defined by

$$S_{zz}(n) = \langle 3\cos^2\theta(n) - 1\rangle/2, \quad (5)$$

is plotted in Fig. 3 together with the *trans* fraction as a function of carbon atom number n, where $\theta(n)$ is the angle between bilayer normal and a line connecting $n - 1$ and $n + 1$th carbon atoms. Because a dihedral angle is defined by successive four carbon atoms, the *trans* fraction is plotted against a half-integer number representing the center of these four. The order parameter profile is in good agreement with that by van der Ploeg and Berendsen (9) and with that of the hard core repulsion theory by Meraldi (25). It shows a plateau at small *n*s more clearly than that by van der Ploeg and Berendsen because the length of the present lipid chain is longer than theirs. After the plateau, it decreases, i.e., the angle θ becomes large, at a large carbon atom number, n = 8–11. These are in good correspondence with Seelig and Niederberger's experimental result (26) for a decanoate system.

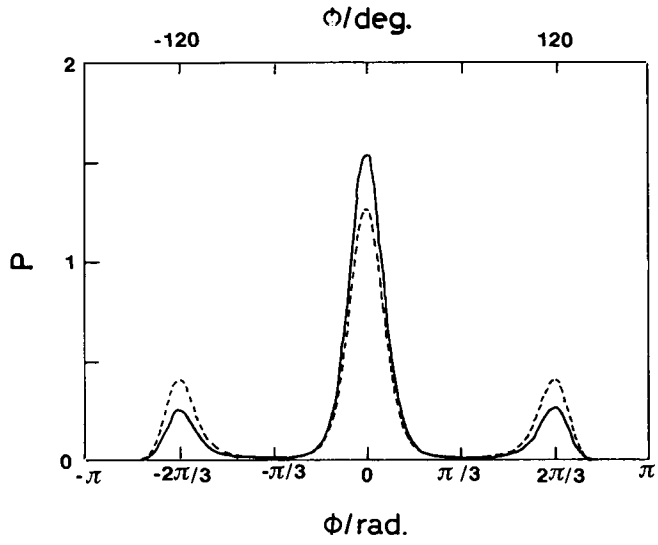

FIGURE 2 Distribution of the dihedral angle of the lauryl chains in the bilayer (——) and in a vacuum (- - -).

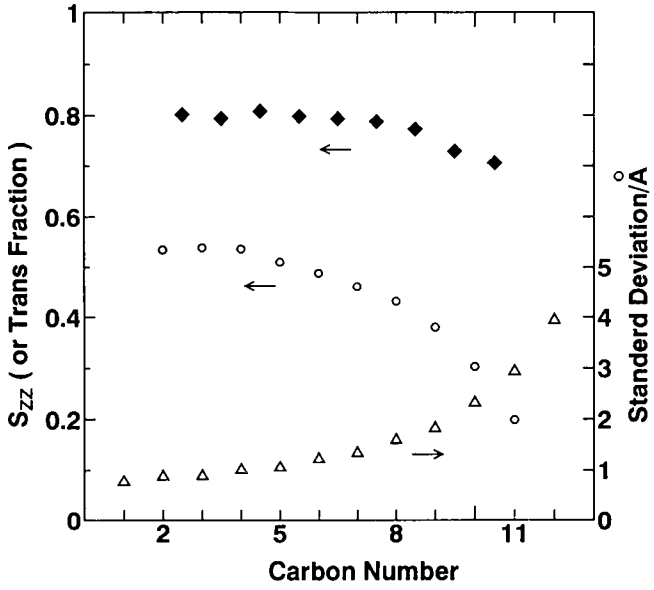

FIGURE 3 Order parameter S_{zz} (○), *trans* fraction (◆), and the standard deviation of the z coordinate of the particle from its averaged position (△) for the lauryl chains in the bilayer.

The figure reveals also that the shape of *trans* fraction as a function of n is conformal to that of the order parameter profile: the order parameter profile must be related to the intramolecular structures of the lipid chain. That is, a decrease in the order parameter is closely related to an increase in the gauche conformation (or a decrease in the *trans* conformation). Conformation of the chain is mainly *trans* between the head group and the middle, whereas a relatively large number of gauche conformations are found near the tail. However, the small number of S_{zz}, i.e., ~0.6, at the plateau can be ascribed to the tilt of the whole chain. The averaged tilt angle of the chain against the bilayer normal is ~30° in this case. We can thus draw a picture of chain in the fluid phase that the chain tilts as a whole from the head group and bends a little at carbon atoms near n = 7–8.

The standard deviation $\sigma_z(n)$ of z coordinate of the carbon atoms from its averaged position, defined by

$$\sigma_z^2(n) = \langle |\bar{z}_n - z_n|^2 \rangle, \qquad (6)$$

is presented in Fig. 3, too, where $\bar{z}_n$ is the averaged z coordinate of nth carbon. This is a measure of delocalization of carbon atom along the z axis. The value is ~1 Å for the head group and is still 1.2 Å for the seventh carbon, and it increases for carbons with the larger numbers to reach ~2 Å for the tail. The fluctuation of the position is small for the plateau carbon atoms, i.e., n = 1–7, and the larger the carbon is, i.e., for n = 8–12, the larger the degree of delocalization along the z axis. This implies that the bend of the chain at n = 7–8 is not a static or solid one but a dynamic or flexible one whose motion is considerably slow.

A kink has been often discussed as an important conformation that facilitates chain packing in the bilayer. Fig. 4 shows the number of kinks per carbon atom. Carbon atom number n in the figure represents the central dihedral angle of the three successive ones that form a kink, i.e., g^+tg^- or g^-tg^+. The number is half-integer in the same way as in Fig. 3. The kink density is 0.03–0.05, the value decreasing with increasing n. Although an odd-even effect (11) appears to exist, it is not definite because of the possibility of statistical error. The averaged number of kinks per chain was 0.27. This is higher than that in a vacuum (0.14), which may be caused by the present lipid molecule of longer chain, i.e., the more spacial degree of freedom. In any case, about a quarter of lipid chain forms a kink, which must make a certain contribution to the stable structure of the lipid bilayer in the fluid phase.

A pair correlation function for particles projected on x-y plane is presented in Fig. 5 for the head groups in the same layer, the tail groups in the same layer, and the tail groups in different layers. First, the figure shows that the lateral structure of the head groups is very similar to that of liquids. The function shows periodic peaks that decay rapidly, i.e., at r = 4.6, 9.2, 13.6, and 17.9 Å with the height of 2.1, 1.3, 1.1, and 1.05, respectively. This implies that the bilayer is at the fluid phase. In this system, however, a long-range correlation is clear compared with the other liquid systems. Even the fifth peak is still clearly observed.

Qualitative structural features found in Fig. 5 are almost the same as those found by Berendsen's group (9): i) the system is in the fluid phase as stated above; ii) the

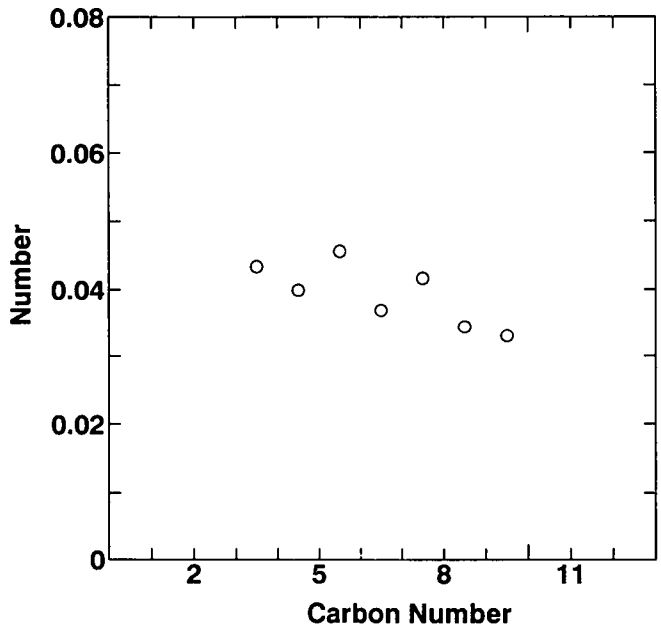

FIGURE 4 Averaged number of kinks per carbon atom, n representing the central carbon atom number of the kink.

tail groups are less correlative than the head groups, probably because of the larger degree of freedom in the space, which is in good correspondence to the result of the standard deviation of z-coordinate; and iii) overlap of the particles on the projected x–y plane is observed even between the tails in the same plane. However, it is interesting that clear correlation is found between the tail groups in the different layers, i.e., small peaks at ~3 and 8 Å, which reveals that interpenetration of the tail group across the layer occurs. The interpenetration is directly observed by perspective pictures shown in Fig. 8 *b*. This is in contrast to the results of van der Ploeg and Berendsen (9), who found no correlation between them, probably because of the small system ($N = 16 \times 2$) or the short chain of lipid molecule. The interpenetration of the chains was predicted first by the theoretical model calculated by Meraldi and Schlitter (8). Our data support the presence of the interpenetration of the chains in the membranes.

Tilt of the molecular axis belongs to a fundamental concept in the discussion of the lipid bilayer structure and its stability. It must be directly related to the order parameter as stated above and to other structural functions such as thickness of the bilayer. The tilt is represented by an angle θ between chain axis and bilayer normal, where the chain axis is defined here by a line connecting the head group and the ninth carbon. The ninth carbon was adopted instead of the tail group to reduce the influence of the molecular bend. The distribution of the tilt angle is presented in Fig. 6. The distribution of the angle formed by the chain axes of the neighboring two molecules is also given in the figure. The "neighbor" was defined as the pair of the molecules whose head groups are nearer to each other than 7.0 Å, i.e., the distance at which the lateral $g(r)$ of the head groups has the first minimum value. The result for the tilt distribution

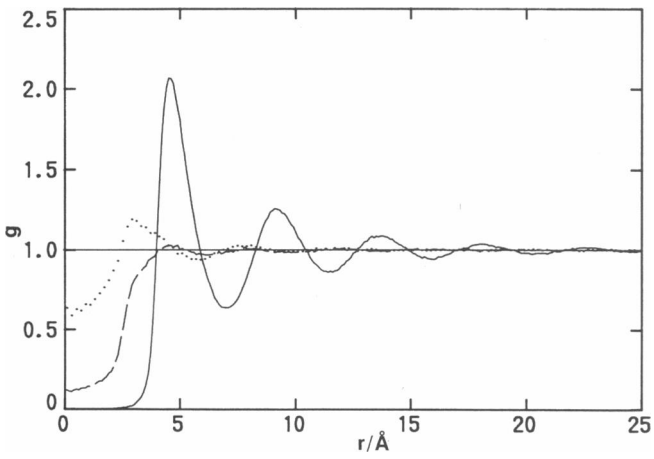

FIGURE 5 Two-dimensional radial distribution function for particular particles. ——, head group–head group in the same layer; – – –, tail group–tail group in the same layer; and · · ·, tail group–tail group in different layers.

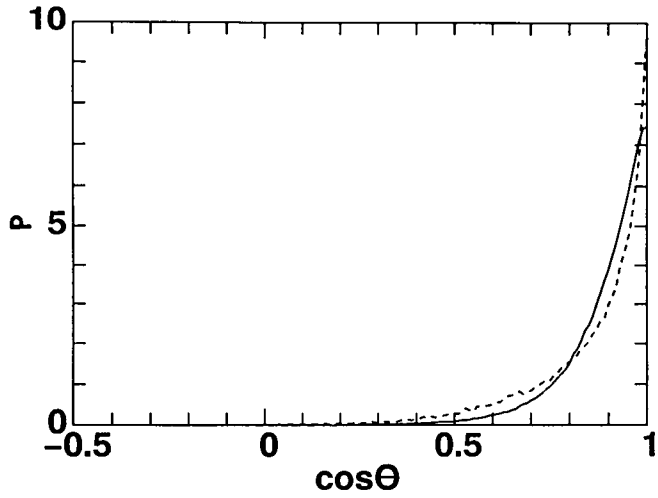

FIGURE 6 Distribution of the tilt angle between the chain axis and the bilayer normal (——), and of the angle formed by the chain axes of the neighboring two molecules (– – –).

was almost the same as that reported by van der Ploeg and Berendsen (9), at least qualitatively. It shows a sharp peak at $\theta = 0°$. The ratio of the chains whose tilt angle less than 30° is as large as 0.71, and 0.28 of the chain has the angle between 30° and 60°, only 1% of the molecules having a larger angle. On the other hand, as shown in the figure, the angle distribution between the neighboring chains is still sharp, i.e., 0.61, 0.35, and 0.04 for $0° \leq \theta \leq 30°$, $30° < \theta < 60°$, and $\theta \geq 60°$, respectively. This indicates that the correlation of the tilt between the neighboring molecules is strong, although the distribution is broader than that of the tilt angle. The averaged tilt angle was 27.5°, which supports the idea that the small order parameter at small carbon numbers is caused mainly by the tilt. The maximum value of the angle formed by the neighboring chain axes was 107°.

Interparticle distance distribution in one molecule is defined as

$$P^n(r) = \left\langle \sum_i \delta(r_i^n - r) \right\rangle, \qquad (7)$$

where r^n is the distance between two particles separated by n bonds. The results are shown in Fig. 7 for $n = 2$–11. From the definition, $P^1(r)$ is a delta function, as the bond length was fixed to r_0 by the SHAKE method. $P^2(r)$ reflects only the C—C—C bending motion, which shows only one sharp peak at $r = (2/3)\sqrt{6}r_0$. Two peaks are found in $P^3(r)$; it is clear from the value of r that the larger one is based on *trans* conformation and the smaller one on gauche conformation, the integrated values being in good agreement with the value from Figs. 1 and 2. The line shape of the peaks must be caused by both the bending motion of C—C—C angle and the libration of dihedral angle within *trans* or gauche conformation, the width being roughly the convolution of these two. The gauche peak is twice as broad as the *trans* one,

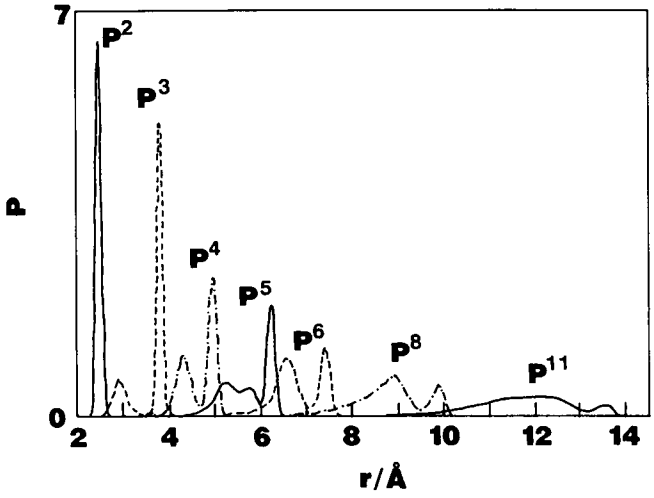

FIGURE 7 Intramolecular interparticle distance distribution $P^n(r)$, two particles being separated by n bonds.

which, however, may be caused only by the geometrical relation between the distance r and the dihedral angle. It is interesting that the relative position of the particle that participates to form gauche conformation is delocalized over as wide as ~1 Å at maximum. In $P^4(r)$, two peaks are found in the figure, too. The right sharp peak must correspond to *tt* (two successive *trans* conformations), and the left broad one to *tg* (indistinguishable from *gt*). $g^{\pm}g^{\pm}$ conformation, which should appear at r = 3.3 Å, was too small to be found in the figure.

In the case of the function $P^5(r)$ there are three peaks in the figure. The right peak represents *ttt* conformation, the center *tgt*, and the left *gtt*. A small peak based on the kink conformation, i.e., g^+tg^- or g^-tg^+, must be merged into the last one. The peak of *tgt* and *gtt* conformations are clearly separated in this case, whose fractions and the distributions are in the same order. However, peaks based on many kinds of combinations of *t* and *g*, including at least one gauche conformation, i.e., the peaks on the lefthand side, merged into each other for n larger than 5, where they are not separately found and the distribution becomes as wide as 2–5 Å. On the other hand, height of the peaks of $P^n(r)$ for all *trans* conformations decays exponentially with increasing n. It shows that the fraction of the chain with all *trans* conformation was only ~0.1, i.e., area of the right peak of $P^{11}(r)$.

Single molecular properties of the lipid in the fluid phase have thus far been investigated by clearly defined statistical mechanical functions. Hereafter, some collective structure will be roughly discussed from the direct observation of the bilayer. Fig. 8 *a* shows projection of the lipids at t = 390 ps onto x-y plane, where only the head and tail groups are presented; each circle represents the head group and the line is drawn between the head group and the tail. Length of this line thus represents a tilt angle of the chain, i.e., the shorter the line is, the smaller the tilt angle. The system is in the disordered phase as discussed in terms of the pair correlation functions. However, it is remarkable that there certainly exist somewhat ordered domains in the system, where direction and tilt of the chains are aligned as indicated by broken lines in the figure. The ordered aggregates are relatively small, the number of the constituents being less than 10. Outside the ordered domains, the chains are randomly directed and tilted. In the fluid phase, thus, the ordered domains or clusters of lipid molecules are dispersed in the disordered "solvent." This can possibly be measured by neutron or x-ray small angle diffraction and Rayleigh scattering of light. Similar phenomena have already been observed, in general, for a number of polymer systems.

Fig. 8 *b* shows a *y*–*z* projection of carbon atoms at t = 390 ps. A lipid molecule is drawn by a small circle representing a head group and lines connecting adjacent car-

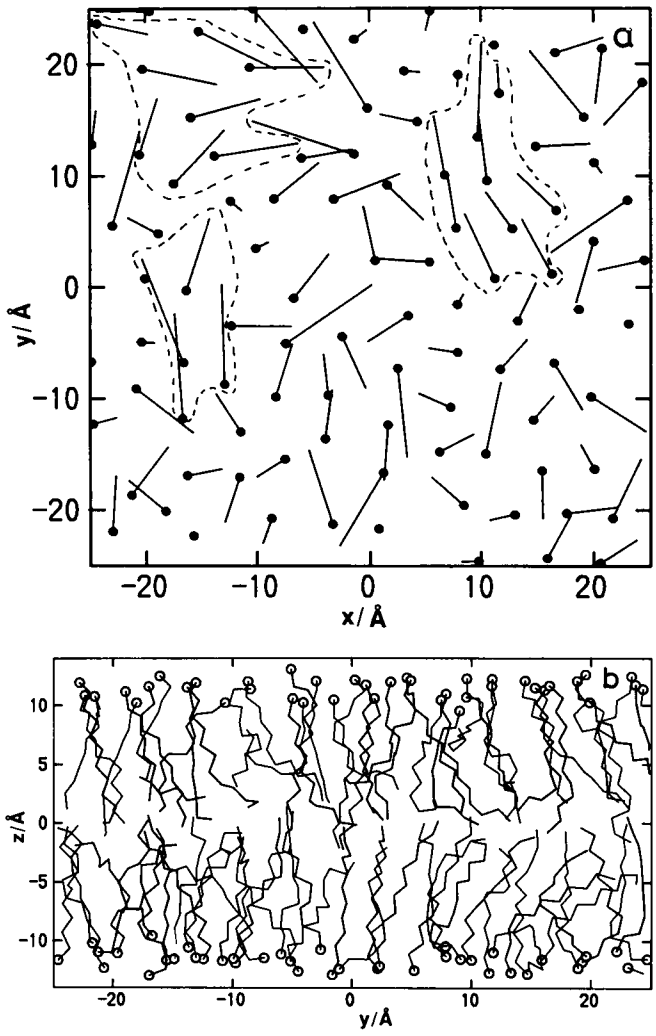

FIGURE 8 (*a*) An *x*–*y* projection of the head and tail groups at t = 390 ps. The circles represent the head particles, and the straight lines connect the head and the tail. (*b*) A *y*–*z* projection of the arbitrarily chosen 80 chain molecules at t = 390 ps. The small circles represent the head groups.

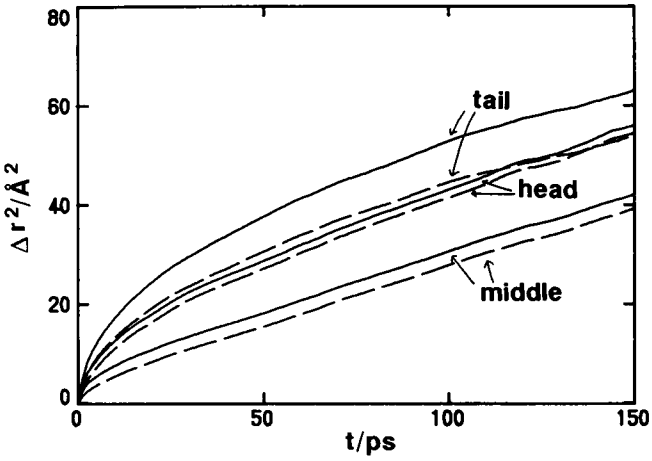

FIGURE 9 Three-dimensional (——) and two-dimensional (- - -) mean square displacements of the head, middle, and tail groups of the chain.

bons successively. Only 80 molecules among 200 are drawn to avoid too much overlap of the lines. The chains tilt and bend in various ways, resulting in the distribution functions stated above. Disordered characters are clear from this figure, too. Interestingly, interpenetrations of chains are clearly shown. Many of the tail groups belonging to different layers are on the same plane, while some of them penetrate to another layer by an order of one or even two bond lengths.

Dynamic properties

Two kinds of mean square displacements of the head, tail, and middle groups are presented in Fig. 9. One is a usual three-dimensional displacement and another two-dimensional one projected on the x–y plane. All the functions rise up rapidly at small t owing to localized libration, after which they give straight lines. These indicate that they are in the stationary states and duration time of the present MD calculation is long enough to analyze the translational motion of this large lipid molecule.

The slopes of the functions are almost the same between the three-dimensional motion and its projected two-dimensional one, which is consistent with the fact that the lipid molecule does not diffuse along z-axis. The initial rise of the curves is larger for three-dimensional motion than for the projected one. The difference is largest for the tail. This means that the libration of the particles along the z-axis is large, in particular, for the tail. This must be closely related to the behavior of the mean square deviation of particles as a function of carbon number n.

Lateral self-diffusion coefficients for the projected motion on the x–y plane were estimated from the slope of the mean square displacements. These were 7.2, 7.1, and 6.2×10^{-6} cm^2/s for the head, tail, and middle groups, respectively. It is reasonable that the values are just $^3/_2$ of those defined as three-dimensional diffusion. These values are smaller than the value $1\text{–}2 \times 10^{-5}$ cm^2/s calculated by van der Ploeg and Berendsen (9) for the smaller system of the shorter calculation. However, the present value is still a little greater than the experimental one (27), i.e., 1.3×10^{-6} cm^2/s. As van der Ploeg and Berendsen (9) pointed out, this may be caused by the fact that there was no water molecule in the calculation that interferes with lateral diffusion of lipid molecule by interaction with its head group. However, the values are satisfactory enough to mimic the diffusion process, because the accuracy of the calculation (and the experiment) is in the order of the value itself.

To examine the translational motion in more detail, we drew trajectories of some head and tail groups by projecting them onto x-y plane. The trajectories of 210 ps are presented in Fig. 10 for arbitrarily chosen seven molecules. The hatched area in the figure corresponds to the averaged occupancy of one molecule, i.e., 25 Å^2, calculated from surface density. It is obvious that moving areas of both head and tail groups are much greater than the hatched one, showing that the motion of the chain is very active.

In particular, the motion of the molecule indicated by the arrow in the figure is interesting. At first, the head group moved about within site B for ~30 ps. Then, it jumped in 5 ps from site B to site C, where it librated for ~45 ps. Then, it jumped back again to site B in 5 ps and stayed there for 25 ps this time. Next it moved suddenly to site A and stayed there for 25 ps. It transferred from site A to site B in ~10 ps and stayed around the site for 50 ps. Thus, a series of the motion can be described in terms of a successive jump between clearly defined sites, and a stay there for a while rather than of hydrodynamic continuous motion. In a certain period, localized and delocalized particles are simultaneously observed.

In the remaining part of this section, one-particle dynamics will be examined to investigate, in particular, how many and what kind of motions exist in lipid chain in the fluid phase.

Velocity autocorrelation functions $C_v(t)$ of the head and tail groups are shown in Fig. 11. The functions show i) rapid cross with 0 value at a few tenths of picoseconds; ii) very fast but small oscillation throughout the time, i.e., 0.07 ps for both particles; iii) somewhat longer oscillatory behavior, the periods being 1.0 and 0.7 ps for the head group and the tail, respectively; and iv) slow return to start oscillation around 0 value, i.e., ~4 and 3 ps for the head and the tail, respectively. The first and second phenomena must be caused by the bending motion with regard to C—C—C bond angle. The third one may represent the libration of single dihedral angle. The difference between the head and the tail may possibly occur owing to the difference in the packing condition, in other words, the free space. The last one may be related to the

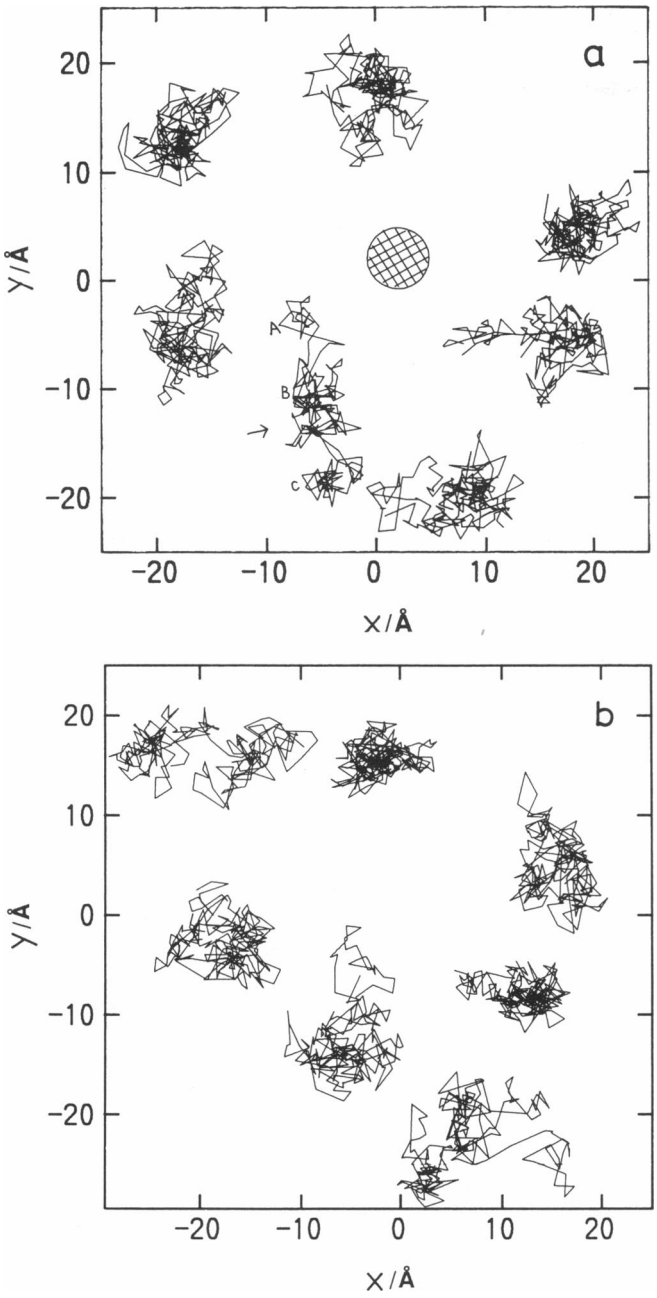

FIGURE 10 Trajectories of the head groups (*a*) and the tail (*b*) of the arbitrarily chosen seven molecules projected on the *x*–*y* plane. The total duration was 210 ps. For *A*, *B*, and *C*, see the text.

translationally localized libration, which contributes to the initial rise of mean square displacement.

A time autocorrelation function $C_r^n(t)$,

$$C_r^n(t) = \langle \mathbf{r}^n(t) \cdot \mathbf{r}^n(0) \rangle / \langle \mathbf{r}^n(0)^2 \rangle, \qquad (8)$$

was defined to investigate more extended motion of particles, which may be described, too, by combinations of dihedral angles, where $\mathbf{r}^n$ represents a vector formed by two carbon atoms separated by n successive C—C bonds. The calculated functions are shown in Fig. 12 for several

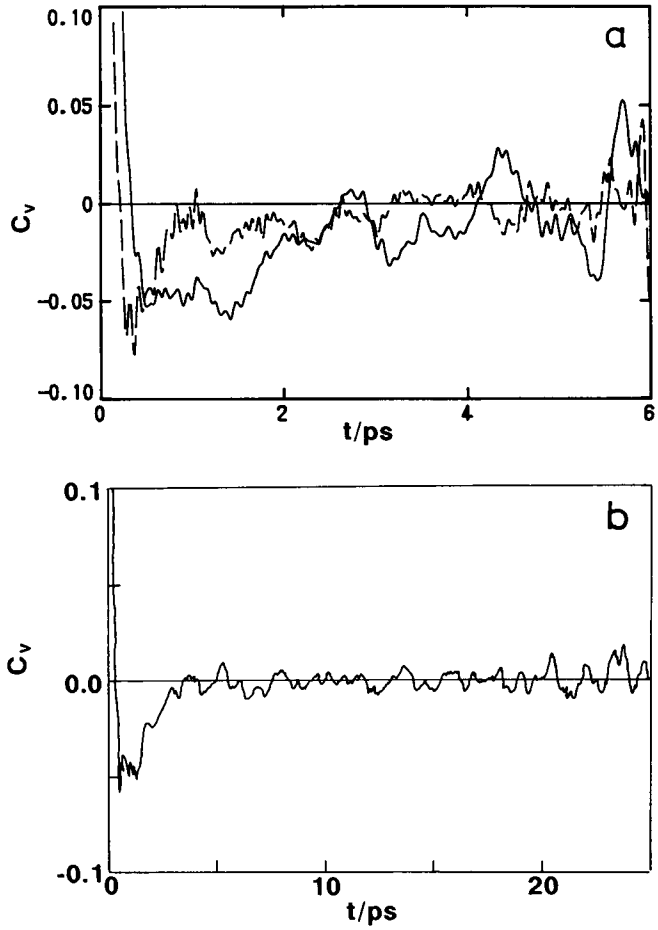

FIGURE 11 (*a*) Short-time and (*b*) long-time velocity autocorrelation function $C_v(t)$ of the head (——) and tail (- - -) groups of the chain molecules.

*n*s. They show exponential-like decay, whose rate becomes longer with increasing *n* value. $C_r^n(t)$ with $n = 4$ and with $n = 7$–10 lies between the curves for $n = 3$ and 5

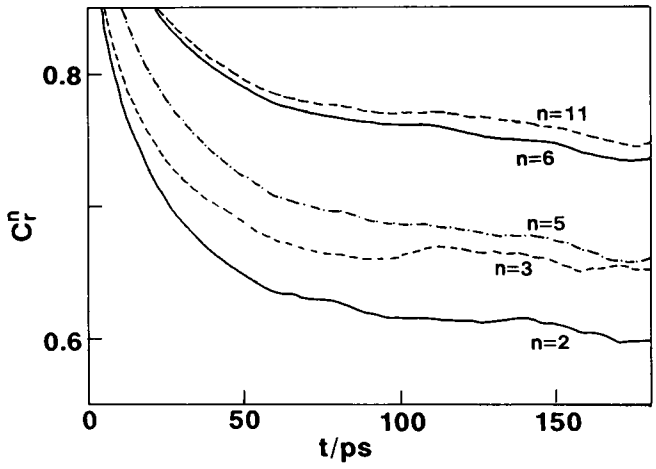

FIGURE 12 Time correlation function $C_r^n(t)$ of the intramolecular vector between two carbon atoms separated by *n* bonds.

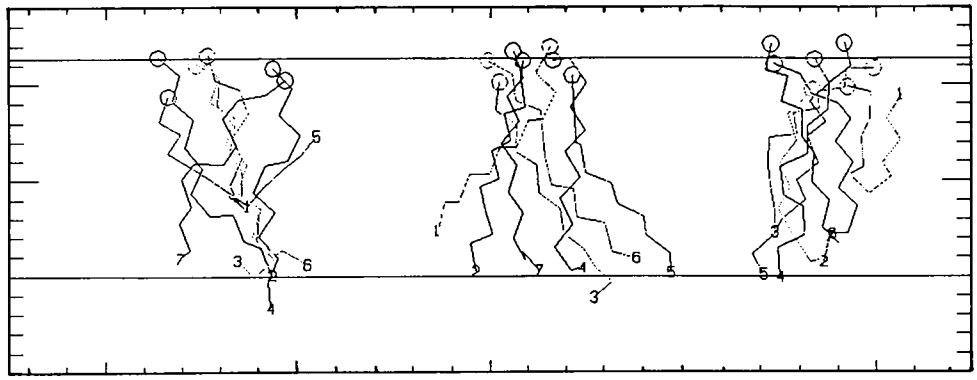

FIGURE 13 Perspective pictures of the lipid chain motion of the arbitrarily chosen three molecules. The trajectories were drawn every 30 ps and the total duration was 180 ps.

and for $n = 6$ and 11, respectively, although they are not shown in the figure. The functions are thus, classified into three groups according to their decay rate. The first one consists of only one function, i.e., $n = 2$; the second is composed of the functions with $n = 3$–5; and the last of those with $n = 6$–11. It is clearly shown that the decay becomes smaller with increasing n. From the definition, large motion is required for the function with large n to make a given increment. However, it is impossible to make such large motion in the dense phase. Thus, the larger the number n becomes, the smaller the decay of the function is. The limiting value of $C^2(t)$ in a vacuum is $(1 - \cos 109.5°)/2 = 0.66\cdots$ when we assume that the origin of vector $\mathbf{r}^n$ is fixed. As shown in the figure, the function decays very rapidly and approaches to a limiting value in ~60 ps. Because $C^3(t)$ represents the motion of particle around one C—C bond, it was proved that the relaxation time of the single dihedral angle is ~60 ps. For larger n, because the motion of the particle should be described by combinations of dihedral angles, the situation becomes very complicated. In any case, it is interesting that the correlation functions can be classified into three groups, although the reason is not clear in the present stage of the analysis. Fig. 13 presents a trajectory of the configuration of selected lipid molecule. As shown in the figure, bend of chain, which leads to a large motion of particles, sometimes takes place. The chain in the figure bent twice in 180 ps. The frequency is, in general, low, depending on the particles in this short period.

Conclusion

Molecular dynamics calculation of the lauryl alcohol–laurate bilayer has been performed using Berendsen's surface-constrained model, the fluid phase being successfully reproduced.

The tilt and bend of the chain plays an important role in the bilayer structure, including behavior of the order parameter. Interpenetration of the layers, as well as formation of collectively ordered small domains, was also found.

The calculated lateral diffusion coefficient was in satisfactory agreement with the experimental one. Successive jumps of the head group, rather the hydrodynamic continuous motion, were observed. Between the jumps, the molecule librated in a local site. Time-dependent autocorrelation functions showed evidence of several different modes of the chain motion, whose time constant ranged from a few tenths of picoseconds to several tens of picoseconds.

We thank the Computer Center of the Institute for Molecular Science and the High Energy Physics Institute for the use of the HITAC S-820 computers. We gratefully acknowledge partial support of this work by a Grant-in-Aid for Scientific Research on Priority Area of "Molecular Approach to Nonequilibrium Process in Solutions" (No. 03231103) from the Ministry of Education, Science and Culture, Japan.

Received for publication 28 September 1992.

REFERENCES

1. Boggs, J. M. 1987. Lipid intermolecular hydrogen bonding: influence on structural organization and membrane function. *Biochim. Biophys. Acta.* 906:353–404.
2. Cameron, D. G., H. L. Casal, and H. H. Mantsch. 1980. Characterization of the pretransition in 1,2-dipalmitoyl-sn-glycero-3-phosphocholine by Fourier transform infrared spectroscopy. *Biochemistry.* 19:3665–3672.
3. Seelig, J., and A. Seelig. 1980. Lipid conformation in model membranes and biological membranes. *Q. Rev. Biophys.* 13:19–61.
4. Herbette, L., C. A. Napolitano, and R. V. McDaniel. 1984. Direct determination of the calcium profile structure for dipalmitoyllecithin multilayers using neutron diffraction. *Biophys. J.* 46:677–685.
5. Marcelja, S. 1974. Chain ordering in liquid crystals. II. Structure of bilayer membranes. *Biochim. Biophys. Acta.* 367:165–176.
6. Gruen, D. W. R. 1980. A statistical mechanical model of the lipid bilayer above its phase transition. *Biochim. Biophys. Acta.* 595:161–183.
7. Meraldi, J.-P., and J. Schlitter. 1981. A statistical mechanical treatment of fatty acyl chain order in phospholipid bilayers and correlation with experimental data. A. Theory. *Biochim. Biophys. Acta.* 645:183–192.
8. Meraldi, J.-P., and J. Schlitter. 1981. A statistical mechanical treatment of fatty acyl chain order in phospholipid bilayers and

correlation with experimental data. B. Dipalmitoyl-3-sn-phosphatidylcholine. *Biochim. Biophys. Acta.* 645:193–210.

9. van der Ploeg, P., and H. J. C. Berendsen. 1982. Molecular dynamics simulation of a bilayer membrane. *J. Chem. Phys.* 76:3271–3276.
10. van der Ploeg, P., and H. J. C. Berendsen. 1982. Molecular dynamics of a bilayer membrane. *Mol. Phys.* 49:233–248.
11. Egberts, E., and H. J. C. Berendsen. 1988. Molecular dynamics simulation of a smectic liquid crystal with atomic detail. *J. Chem. Phys.* 89:3718–3732.
12. Biswas, A., and B. L. Schürmann. 1991. Molecular dynamics simulation of a dense model bilayer of chain molecules with fixed head groups. *J. Chem. Phys.* 95:5377–5386.
13. Raghavan, K., M. R. Reddy, and M. L. Berkowitz. 1992. A molecular dynamics study of the structure and dynamics of water between dilauroylphosphatidylethanolamine bilayers. *Langmuir.* 8:233–240.
14. Hockney, R. W. 1970. The potential calculation and some applications. *Methods Comp. Phys.* 9:135–211.
15. Ryckaert, J. P., G. Cicotti, and H. J. C. Berendsen. 1977. Numerical integration of the Cartesian equations of motion of a system with constraints: molecular dynamics of n-alkanes. *J. Comp. Phys.* 23:327–341.
16. Seelig, J. 1977. Deuterium magnetic resonance: theory and application to lipid membranes. *Q. Rev. Biophys.* 10:353–418.
17. Berendsen, H. J. C., J. P. M. Postoma, W. F. van Gunsteren, A. DiNola, and J. R. Haak. 1984. Molecular dynamics with coupling to an external bath. *J. Chem. Phys.* 81:3684–3690.
18. Weber, T. A. 1979. Relaxation of n-octane fluid. *J. Chem. Phys.* 70:4277–4284.
19. Ryckaert, J. P., and A. Bellemans. 1978. Molecular dynamics of liquid alkane. *Faraday Discuss. Chem. Soc.* 66:95–106.
20. Ryckaert, J. P., and A. Bellemans. 1975. Molecular dynamics of liquid n-butane near its boiling point. *Chem. Phys. Lett.* 30:123–125.
21. Gibson, K. D., and H. A. Scheraga. 1967. Minimization of polypeptide energy. I. Preliminary structures of bovine pancreatic ribonuclease S-peptide. *Proc. Natl. Acad. Sci. USA* 58:420–427.
22. Warme, P. K., and H. A. Scheraga. 1973. Refinement of X ray data on proteins. II. Adjustment of structure of specified geometry to relieve atomic overlaps. *J. Comp. Phys.* 12:49–64.
23. Marsh, D. 1974. Statistical mechanics of the fluidity of phospholipid bilayers and membranes. *J. Membr. Biol.* 18:145–162.
24. Padrilla, P., and S. Toxvaerd. 1991. Structure and dynamical behavior of fluid n alkanes. *J. Chem. Phys.* 95:509–519.
25. Meraldi, J.-P. 1981. Comments on the use of the order parameters obtained from ^{2}H-NMR to describe the anisotropic motions of the methylene groups of the fatty acyl chains in lipid bilayer membrane. *Chem. Phys. Lipids.* 28:227–239.
26. Seelig, J., and W. Niederberger. 1974. Two pictures of a lipid bilayer. A comparison between deuterium label and spin-label experiments. *Biochemistry.* 13:1585–1588.
27. Schindler, H., and J. Seelig. 1974. EPR spectra of spin labels in lipid bilayers. II. Rotation of steroid spin probes. *J. Chem. Phys.* 61:2946–2949.